Inorg. Chem. **2008**, *47*, 4471−4480

Synthesis and Properties of Diphenoxo-Bridged Co^{II}, Ni^{II}, Cu^{II}, and Zn^{II} Complexes of a New Tripodal Ligand: Generation and Properties of M^{II}-Coordinated Phenoxyl Radical Species

Atasi Mukherjee,[†] Francesc Lloret,[‡] and Rabindranath Mukherjee*[,†]

Department of Chemistry, Indian Institute of Technology Kanpur, Kanpur 208 016, India, and Departament de Química Inorgànica/Instituto de Ciencia Molecular (ICMOL), Universitat de València, Polígono de la Coma, s/n, 46980-Paterna (València), Spain

Received June 29, 2007

Four dinuclear complexes of composition $[M^{II}_2(L)_2]\cdot xS$ [M = Co, x = 0.5, S = 1,4-dioxane (**1**·0.5 1,4-dioxane); Ni, x = 0 (**2**) [single crystals have x = 2, S = diethyl ether (**2**·2 diethyl ether)]; Cu, x = 0 (**3**); Zn, x = 0.5, S = 1,4-dioxane (**4**·0.5 1,4-dioxane)] have been synthesized using a new tripodal ligand [2,4-di*tert*-butyl-6-{[(2-pyridyl)ethyl](2-hydroxybenzyl)-aminomethyl}-phenol (H_2L)], in its deprotonated form, providing a N_2O_2 donor set. Crystallographic analyses reveal that the complexes have a similar diphenoxo-bridged structure. Each metal ion is terminally coordinated by 2,4-di*tert*-butyl-phenolate oxygen, a tertiary amine, and a pyridyl nitrogen. From each ligand, unsubstituted phenolate oxygen provides bridging coordination. Thus, each metal center assumes $M^{II}N_2O_3$ coordination. Whereas the geometry around the metal ion in **1**·0.5 1,4-dioxane, **2**·2 diethyl ether and, **4**·0.5 1,4-dioxane is distorted trigonal-bipyramidal, in **3** each copper(II) center is in a square-pyramidal environment. Temperature-dependent magnetic behavior has been investigated to reveal intramolecular antiferromagnetic exchange coupling for these compounds ($-J$ = 6.1, 28.6, and 359 cm^{-1} for **1**·0.5 1,4-dioxane, **2**, and **3**, respectively). Spectroscopic properties of the complexes have also been investigated. When examined by cyclic voltammetry (CV), all four complexes undergo in CH_2Cl_2 two reversible ligand-based (2,4-di*tert*-butylphenolate unit) one-electron oxidations [$E_{1/2}^1$ = 0.50−0.58 and $E_{1/2}^2$ = 0.63−0.75 V vs SCE (saturated calomel electrode)]. The chemically/coulometrically generated two-electron oxidized form of **3** rearranges to a monomeric species with instantaneous abstraction of the hydrogen atom, and for **4**·0.5 1,4-dioxane the dimeric unit remains intact, exhibiting an EPR spectrum characteristic of the presence of Zn^{II}-coordinated phenoxyl radical (UV−vis and EPR spectroscopy). To suggest the site of oxidation (metal or ligand-centered), in each case DFT calculations have been performed at the B3LYP level of theory.

Introduction

Formation of the tyrosyl radical in mononuclear copper enzyme galactose oxidase,[1] a prototypical example of a class of metalloproteins to use free radicals as cofactors to promote oxidation reactions,[1b,2,3] has triggered current research interest in the preparation and studies of metal-coordinated phenoxyl radicals.[4−11] For a better understanding of the M^{II}-tyrosyl radical species in the formation and its subsequent stability/reactivity, we describe herein diphenoxo-bridged complexes of M^{II} ions (cobalt, nickel, copper, and zinc) of a new phenol-based tetradentate ligand H_2L [comprising of two phenol groups (one unsubstituted, and the other with 2,4-di*tert*-butyl substituents), an ethylpyridine unit, and an aliphatic amine], and their two-electron oxidized counterparts. Specifically, we present a comprehensive report on the

* To whom correspondence should be addressed. Tel.: +91-512-2597437. Fax: +91-512-2597436. E-mail: rnm@iitk.ac.in.
† Indian Institute of Technology Kanpur.
‡ Universitat de València.

(1) (a) Klinman, J. P. *Chem. Rev.* **1996**, *96*, 2541–2561. (b) Stubbe, J.; van der Donk, W. A. *Chem. Rev.* **1998**, *98*, 705–762. (c) Krüger, H. J. *Angew. Chem., Int. Ed.* **1999**, *38*, 627–631. (d) Itoh, S.; Taki, M.; Fukuzumi, S. *Coord. Chem. Rev.* **2000**, *198*, 3–20. (e) Jazdzewski, B. A; Tolman, W. B. *Coord. Chem. Rev.* **2000**, *200−202*, 633–685. (f) Chaudhuri, P.; Wieghardt, K. *Prog. Inorg. Chem.* **2001**, *50*, 151–216. (g) Whittaker, J. W. *Chem. Rev.* **2003**, *103*, 2347–2363. (h) Tolman, W. B. In *Comprehensive Coordination Chemistry-II: From Biology to Nanotechnology*; McCleverty, J. A., Meyer, T. J., Que, L., Jr., Tolman, W. B., Eds.; Elsevier/Pergamon: Amsterdam, 2004; *Vol. 8*, pp 715−737. (i) Thomas, F. *Eur. J. Inorg. Chem.* **2007**, 2379–2404.
(2) Stubbe, J. *Chem. Commun.* **2003**, 2511–2513.
(3) Limberg, C. *Angew. Chem., Int. Ed.* **2003**, *42*, 5932–5954.

10.1021/ic701283b CCC: $40.75
Published on Web 05/08/2008

synthesis, crystal structure, magnetic behavior, redox chemistry, and studies on generation and stability/properties of M^{II}-coordinated phenoxyl radical species. It is appropriate to mention here a few noteworthy aspects of the present complexes of phenol-based tetradentate N_2O_2 donor ligand with respect to that reported in the literature.[1i] (i) To the best of our knowledge, there is no report in the literature on structurally characterized monomeric/dimeric Cu^{II} complexes that bear a phenol unit without steric bulk at its ortho position. The present ligand is unique due to its unsymmetrical nature. (ii) Only few reports concerning the oxidation behavior of the phenolate complexes of tripodal N_2O_2 donor set exist. (iii) The instability of phenoxyl radical complexes, as observed in this work, is common to reported systems with the N_2O_2 donor set. In fact, compared to N_3O donor ligands, the phenoxyl radical complexes with N_2O_2 donor ligands are less stable. (iv) The hydrogen atom abstraction chemistry implied in this work is noteworthy, considering reported dicopper(II) systems with N_2O_2 ligands. To throw light on the site of oxidation (metal or ligand-centered), in each case DFT calculations have been performed at the B3LYP level of theory.

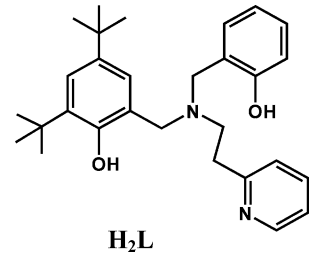

H_2L

Experimental Section

Materials and Reagents. All reagents were obtained from commercial sources and used as received. Solvents were dried/purified as reported previously.[12] The precursors 2,4-di*tert*-butyl-6-(hydroxymethyl)phenol,[13] 2,4-di*tert*-butyl-6-(chloromethyl)phenol,[14] and 2-((2-(2-pyridinyl)ethylamino)methyl)phenol[15] for the synthesis of H_2L, and tetra-*n*-butylammonium perchlorate (TBAP)[12a]were prepared following literature procedures. Zinc(II) perchlorate hexahydrate was prepared from the reaction between $ZnCO_3$ and aqueous $HClO_4$.

Ligand Synthesis. 2,4-di*tert*-butyl-6-{[(2-pyridyl)ethyl](2-hydroxybenzyl)amino-methyl}-phenol ($H_2L \cdot$1,4-Dioxane). To a magnetically stirred mixture of 2-((2-(2-pyridinyl)ethylamino)-methyl)phenol (1.74 g, 7.65 mmol) and Et_3N (3.49 mL, 25.0 mmol) in 1,4-dioxane (6 mL), a solution of 2,4-di*tert*-butyl-6-(chloromethyl)phenol (1.95 g, 7.65 mmol) in 1,4-dioxane (4 mL) was added dropwise. The resulting orange reaction mixture was allowed to stir for 90 min at 298 K. It was then heated (~60 °C), and an additional amount of Et_3N (5.23 mL, 37.5 mmol) was added portionwise over a period of 2 h. The pH of the mixture was maintained below 10 during this addition. The resulting solution was then cooled to 40 °C, filtered, and the filtrate was evaporated

(4) (a) Wang, Y.; Stack, T. D. P. *J. Am. Chem. Soc.* **1996**, *118*, 13097–13098. (b) Wang, Y.; DuBois, J. L.; Hedman, B.; Hodgson, K. O.; Stack, T. D. P. *Science* **1998**, *279*, 537–540. (c) Storr, T.; Wasinger, E. C.; Pratt, R. C.; Stack, D. P. *Angew. Chem., Int. Ed.* **2007**, *46*, 5198–5201.

(5) (a) Sokolowski, A.; Leutbecher, H.; Weyhermüller, H.; Schnepf, R.; Bothe, E.; Bill, E.; Hildebrandt, P.; Wieghardt, K. *J. Biol. Inorg. Chem.* **1997**, *2*, 444–453. (b) Müller, J.; Weyhermüller, T.; Bill, E.; Hildebrandt, P.; Ould-Moussa, L.; Glaser, T.; Wieghardt, K. *Angew. Chem., Int. Ed.* **1998**, *37*, 616–619. (c) Chaudhuri, P.; Hess, M.; Flörke, U.; Wieghardt, K. *Angew. Chem., Int. Ed.* **1998**, *37*, 2217–2220. (d) Chaudhuri, P.; Hess, M.; Weyhermüller, T.; Wieghardt, K. *Angew. Chem., Int. Ed.* **1999**, *38*, 1095–1098. (e) Chaudhuri, P.; Hess, M.; Müller, J.; Hildenbrand, K.; Bill, E.; Weyhermüller, T.; Wieghardt, K. *J. Am. Chem. Soc.* **1999**, *121*, 9599–9610. (f) Kruse, T.; Weyhermüller, T.; Wieghardt, K. *Inorg. Chim. Acta* **2002**, *331*, 81–89.

(6) (a) Zurita, D.; Scheer, C.; Pierre, J. L.; Saint-Aman, E. *J. Chem. Soc., Dalton Trans.* **1996**, 4331–4336. (b) Zurita, D.; Gautier-Luneau, I.; Ménage, S.; Pierre, J. L.; Saint-Aman, E. *J. Bio. Inorg. Chem.* **1997**, *2*, 46–55. (c) Thomas, F.; Gellon, G.; Gautier-Luneau, I.; Saint-Aman, E.; Pierre, J. L. *Angew. Chem., Int. Ed.* **2002**, *41*, 3047–3050. (d) Philibert, A.; Thomas, F.; Philouze, C.; Hamman, S.; Saint-Aman, E.; Pierre, J. L. *Chem.—Eur. J.* **2003**, *9*, 3803–3812. (e) Michel, F.; Thomas, F.; Hamman, S.; Saint-Aman, E.; Bucher, C.; Pierre, J. L. *Chem.—Eur. J.* **2004**, *10*, 4115–4125. (f) Michel, F.; Torelli, S.; Thomas, F.; Duboc, C.; Philouze, C.; Belle, C.; Hamman, S.; Saint-Aman, E.; Pierre, J. L. *Angew. Chem., Int. Ed.* **2005**, *44*, 438–441. (g) Michel, F.; Thomas, F.; Hamman, S.; Philouze, C.; Saint-Aman, E.; Pierre, J. L. *Eur. J. Inorg. Chem.* **2006**, 3684–3696. (h) Rotthaus, O.; Jarjayes, O.; Thomas, F.; Philouze, C.; Saint-Aman, E.; Pierre, J. L. *Dalton Trans.* **2007**, 889–895.

(7) (a) Shimazaki, Y.; Huth, S.; Hirota, S.; Yamauchi, O. *Bull. Chem. Soc. Jpn.* **2000**, *73*, 1187–1195. (b) Shimazaki, Y.; Huth, S.; Odani, A.; Yamauchi, O. *Angew. Chem., Int. Ed.* **2000**, *39*, 1666–1669. (c) Shimazaki, Y.; Huth, S.; Hirota, S.; Yamauchi, O. *Inorg. Chim. Acta* **2002**, *331*, 168–170. (d) Shimazaki, Y.; Tani, F.; Fukui, K.; Naruta, Y.; Yamauchi, O. *J. Am. Chem. Soc.* **2003**, *125*, 10512–10513. (e) Shimazaki, Y.; Huth, S.; Karasawa, S.; Hirota, S.; Naruta, Y.; Yamauchi, O. *Inorg. Chem.* **2004**, *43*, 7816–7822. (f) Shimazaki, Y.; Yajima, T.; Tani, F.; Karasawa, S.; Fukui, K.; Naruta, Y.; Yamauchi, O. *J. Am. Chem. Soc.* **2007**, *129*, 2559–2568. (g) Shimazaki, Y.; Kabe, R.; Huth, S.; Tani, F.; Naruta, Y.; Yamauchi, O. *Inorg. Chem.* **2007**, *46*, 6083–6090.

(8) (a) Itoh, S.; Takayama, S.; Arakawa, R.; Furuta, A.; Komatsu, M.; Ishida, A.; Takamuku, S.; Fukuzumi, S. *Inorg. Chem.* **1997**, *36*, 1407–1416. (b) Itoh, S.; Taki, M.; Takayama, S.; Nagatomo, S.; Kitagawa, T.; Sakurada, N.; Arakawa, R. S.; Fukuzumi, S. *Angew. Chem., Int. Ed.* **1999**, *38*, 2774–2776. (c) Itoh, S.; Taki, M.; Kumei, H.; Takayama, S.; Nagatomo, S.; Kitagawa, T.; Sakurada, N.; Arakawa, R. S.; Fukuzumi, S. *Inorg. Chem.* **2000**, *39*, 3708–3711. (d) Taki, M.; Kumei, H.; Itoh, S.; Fukuzumi, S. *J. Inorg. Biochem.* **2000**, *78*, 1–5. (e) Taki, M.; Kumei, H.; Nagatomo, S.; Kitagawa, T.; Itoh, S.; Fukuzumi, S. *Inorg. Chim. Acta* **2000**, *300—302*, 622–632. (f) Taki, M.; Hattori, H.; Osako, T.; Nagatomo, S.; Shiro, M.; Kitagawa, T.; Itoh, S. *Inorg. Chim. Acta* **2004**, *357*, 3369–3381.

(9) Whittaker, M. M.; Duncan, W. R.; Whittaker, J. W. *Inorg. Chem.* **1996**, *35*, 382–386.

(10) (a) Benisvy, L.; Blake, A. J.; Collison, D.; Davies, E. S.; Garner, C. D.; McInnes, E. J. L.; McMaster, J.; Whittaker, G.; Wilson, C. *Chem. Commun.* **2001**, 1824–1825. (b) Benisvy, L.; Blake, A. J.; Collison, D.; Davies, E. S.; Garner, C. D.; McInnes, E. J. L.; McMaster, J.; Whittaker, G.; Wilson, C. *Dalton Trans.* **2003**, 1975–1985. (c) Benisvy, L.; Bill, E.; Blake, A. J.; Collison, D.; Davies, E. S.; Garner, C. D.; Guindy, C. I.; McInnes, E. J. L.; McArdle, G.; McMaster, J.; Wilson, C.; Wolowska, J. *Dalton Trans.* **2004**, 3647–3653. (d) Benisvy, L.; Bill, E.; Blake, A. J.; Collison, D.; Davies, E. S.; Garner, C. D.; McArdle, G.; McInnes, E. J. L.; McMaster, J.; Ross, S. H. K.; Wilson, C. *Dalton Trans.* **2006**, 258–267.

(11) (a) Adams, H.; Bailey, N. A.; Fenton, D. E.; He, Q.; Ohba, M.; Okawa, H. *Inorg. Chim. Acta* **1994**, *215*, 1–3. (b) Vaidyanathan, M.; Viswanathan, R.; Palaniandavar, M.; Balasubramanian, T.; Prabhaharan, P.; Muthiah, T. P. *Inorg. Chem.* **1998**, *37*, 6418–6427.

(12) (a) Ray, M.; Mukerjee, S.; Mukherjee, R. *J. Chem. Soc., Dalton Trans.* **1990**, 3635–3638. (b) Gupta, N.; Mukerjee, S.; Mahapatra, S.; Ray, M.; Mukherjee, R. *Inorg. Chem.* **1992**, *31*, 139–141. (c) Ray, M.; Ghosh, D.; Shirin, Z.; Mukherjee, R. *Inorg. Chem.* **1997**, *36*, 3568–3572. (d) Patra, A. K.; Mukherjee, R. *Inorg. Chem.* **1999**, *38*, 1388–1393.

(13) (a) Sokolowski, A.; Müller, J.; Weyhermüller, T.; Schnepf, R.; Hildebrandt, P.; Hildenbrand, K.; Bothe, E.; Wieghardt, K. *J. Am. Chem. Soc.* **1997**, *119*, 8889–8900. (b) Cepanec, I.; Mikuldaš, H.; Vinković, V. *Syn. Commun.* **2001**, *31*, 2913–2919.

(14) Lanznaster, M.; Hratchiran, H. P.; Heeg, M. J.; Hryhorczuk, L. M.; MacGarvey, B. R.; Schlegel, H. B.; Verani, C. N. *Inorg. Chem.* **2006**, *45*, 955–957.

(15) Tandon, S. S.; Chander, S.; Thompson, L. K.; Bridson, J. N.; McKee, V. *Inorg. Chim. Acta* **1994**, *219*, 55–65.

under reduced pressure. The crude solid thus obtained was recrystallized from a mixture of CH_2Cl_2 and *n*-hexane (1:2, v/v), which afforded a white crystalline solid of $H_2L \cdot$1,4-dioxane (yield: 2.16 g, ~63%). Anal. Calcd for $C_{33}H_{46}N_2O_4$: C, 74.15; H, 8.61; N, 5.24. Found: C, 74.01; H, 8.72; N, 5.18. ^{1}H NMR (80 MHz; $CDCl_3$): δ 8.72 (d, $J_{HH} = 7.80$ Hz, 1H, $H_{6'}$ of py), 6.72−7.82 (m, 9H, $H_{3',4',5'}$ of py and $H_{3,5,3'',4'',5'',6''}$ of PhOH), 3.86 (s, 4H, $-CH_2-$), 3.71 (s, 8H, $-CH_2-CH_2-$ of 1,4-dioxane), 3.16 (t, $J_{HH} = 8.03$ Hz, 2H, $-CH_2-CH_2-$), 2.92 (t, $J_{HH} = 8.40$ Hz, 2H, $-CH_2-CH_2-$), 1.34 (s, 18H, *tert*-butyl).

Synthesis of Metal Complexes. $[Co^{II}_2(L)_2] \cdot$0.5 1,4-Dioxane (1·0.5 1,4-Dioxane). To a magnetically stirred solution of H_2L (0.2 g, 0.448 mmol) in MeOH (8 mL) was added a solution of $Co(OAc)_2 \cdot 4H_2O$ (0.112 g, 0.448 mmol) in MeOH (5 mL) dropwise, and the resulting mixture was refluxed for 1 h. The pink precipitate that formed was collected by filtration, washed with MeOH, and dried in vacuum. The complex was recrystallized by diffusion of diethyl ether into a concentrated solution of the complex in CH_2Cl_2. Pink crystals that obtained (yield: 0.135 g, ~60%) were found to be suitable for X-ray structural study.

Characterization of 1·0.5 1,4-Dioxane. Anal. Calcd for $C_{60}H_{76}Co_2N_4O_5$: C, 68.58; H, 7.24; N, 5.33. Found: C, 68.42; H, 7.15; N, 5.21. IR (KBr, cm^{-1}, selected peak): 1275 ν(C−O) of the phenolate group. Absorption spectrum [λ_{max}, nm (ϵ, M^{-1} cm^{-1})]: (in CH_2Cl_2) 290 (21 000), 380 sh (2900), 550 sh (190), 570 (200), 660 sh (20), 740 (30).

$[Ni^{II}_2(L)_2]$ (2). To a magnetically stirred mixture of H_2L (0.3 g, 0.673 mmol) and Et_3N (0.136 g, 1.346 mmol) in MeOH (10 mL) was added dropwise a solution of $Ni(OAc)_2 \cdot 4H_2O$ (0.167 g, 0.673 mmol) in MeOH (6 mL). The green solid that precipitated was collected by filtration, washed with MeOH, and dried in vacuum (yield: 0.217 g, ~64%). The complex was recrystallized by diffusion of diethyl ether into a concentrated solution of the complex in CH_2Cl_2, affording green crystals with two molecules of diethyl ether as solvent of crystallization $[Ni^{II}_2(L)_2] \cdot 2$ diethyl ether (**2**·2 diethyl ether). Such crystals were suitable for X-ray structural study.

Characterization of 2. Anal. Calcd for $C_{58}H_{72}N_4Ni_2O_4$: C, 69.23; H, 7.16; N, 5.57. Found: C, 69.39; H, 7.25; N, 5.52. IR (KBr, cm^{-1} selected peak): 1275 ν(C−O) of phenolate group. Absorption spectrum [λ_{max}, nm (ϵ, M^{-1} cm^{-1})]: (in CH_2Cl_2) 290 (16 800), 420 (3200), 670 (60), 970 (20).

$[Cu^{II}_2(L)_2]$ (3). To a magnetically stirred solution of H_2L (0.3 g, 0.673 mmol) in MeOH (8 mL), a solution of $Cu(OAc)_2 \cdot H_2O$ (0.134 g, 0.673 mmol) in MeOH (5 mL) was added dropwise. The brown solid that formed was collected by filtration, washed with MeOH, and dried in vacuum. Brown crystals suitable for X-ray structural study were achieved by diffusion of diethyl ether into a concentrated solution of the complex in CH_2Cl_2 (yield: 0.200 g, ~58%).

Characterization of 3. Anal. Calcd for $C_{58}H_{72}Cu_2N_4O_4$: C, 68.57; H, 7.09; N, 5.51. Found: C, 68.66; H, 7.20; N, 5.60. IR (KBr, cm^{-1} selected peak): 1271 ν(C−O) of phenolate group. Absorption spectrum [λ_{max}, nm (ϵ, M^{-1} cm^{-1})]: (in CH_2Cl_2) 290 (17 400), 340 sh (5300), 390 (3400), 510 sh (2200), 760 (410).

$[Zn^{II}_2(L)_2] \cdot$0.5 1,4-Dioxane (4·0.5 1,4-Dioxane). To a magnetically stirred mixture of H_2L (0.2 g, 0.448 mmol) and Et_3N (0.091 g, 0.896 mmol) in MeOH (10 mL), a solution of $[Zn(H_2O)_6][ClO_4]_2$ (0.167 g, 0.448 mmol) in MeOH (7 mL) was added dropwise. The resulting solution was stirred for an hour. Evaporation of this solution afforded light-yellowish solid, which was recrystallized by dissolving in CH_2Cl_2 followed by addition of *n*-hexane. After a few days, white crystals were obtained, which were suitable for X-ray structural study (yield: 0.139 g, ~61%).

Characterization of 4·0.5 1,4-Dioxane. Anal. Calcd for $C_{60}H_{76}N_4O_6Zn_2$: C, 67.80; H, 7.16; N, 5.27. Found: C, 67.71; H, 7.09; N, 5.12. ^{1}H NMR (400 MHz, $CDCl_3$): δ 8.81 (s, 1H, $H_{6'}$ of py), 7.63 (t, $J_{HH} = 7.56$ Hz, 1H, $H_{4'}$ of py), 7.26 (s, 2H, $H_{3,5}$ of $^{t\text{-bu}}$PhO), 7.22 (d, $J_{HH} = 7.96$ Hz, 1H, $H_{3'}$ of py), 7.16 (t, $J_{HH} = 7.80$ Hz, 1H, $H_{5'}$ of py), 6.97 (t, $J_{HH} = 7.50$ Hz, 1H, $H_{4''}$ of PhO), 6.91 (d, $J_{HH} = 7.10$ Hz, 1H, $H_{6''}$ of PhO), 6.83 (d, $J_{HH} = 7.02$ Hz, 1H, $H_{3''}$ of PhO), 6.51 (t, $J_{HH} = 7.23$ Hz, 1H, $H_{5''}$ of PhO), 3.45 (s, 4H, $-CH_2-$), 3.05 (m, 2H, $-CH_2-CH_2-$), 2.17 (m, 2H, $-CH_2-CH_2-$), 1.34 (s, 9 H, 2-*tert*-butyl), 1.18 (s, 9H, 4-*tert*-butyl).

Physical Measurements. Elemental analyses were obtained using a Thermo Quest EA 1110 CHNS-O, Italy. Spectroscopic measurements were made using the following instruments: IR (KBr, 4000−600 cm^{-1}), Bruker Vector 22; electronic, Perkin Elmer Lambda 2 and Agilent 8453 diode-array spectrophotometers. ^{1}H NMR spectra ($CDCl_3$ solution) were obtained on either a Bruker WP-80 (80 MHz) or a JEOL JNM LA (400 MHz) spectrophotometer. Chemical shifts are reported in ppm referenced to TMS. Electrospray ionization LC-MS mass spectra were recorded using a Waters Q Tof Premier micromass HAB 213 mass spectrophotometer. X-band EPR spectra were recorded using a Bruker EMX 1444 EPR spectrometer operating at 9.455 GHz. The EPR spectra were calibrated with diphenylpicrylhydrazyl, DPPH ($g = 2.0037$).

Variable-temperature magnetic susceptibility measurements on polycrystalline samples of **1**·0.5 1,4-dioxane, **2**, and **3** were performed with a Quantum Design (Model MPMSXL-5) SQUID magnetic susceptometer at València, Spain.

Cyclic voltammetric (CV) experiments were performed at 298 K by using a PAR model 370 electrochemistry system consisting of M-174A polarographic analyzer, M-175 universal programmer, and RE 0074 X-Y recorder. The cell contained a Beckman (M 39273) platinum-inlay working electrode, a platinum wire auxiliary electrode, and a saturated calomel electrode (SCE) as a reference electrode. Details of the cell configuration are as described before.[16] For coulometry, a platinum wire-gauze was used as the working electrode. The solutions were ~1.0 mM in complex and 0.1 M in supporting electrolyte TBAP.

Crystal Structure Determination. Single crystals of suitable dimensions were used for data collection. Diffraction intensities were collected on a Bruker SMART APEX CCD diffractometer, with graphite-monochromated Mo Kα (0.71073 Å) radiation at 100(2) K. The data were corrected for absorption. The structures were solved by *SIR-97*, expanded by Fourier-difference syntheses, and refined with the *SHELXL-97* package incorporated into the *WinGX 1.64* crystallographic package.[17] The position of the hydrogen atoms were calculated by assuming ideal geometries but not refined. All non-hydrogen atoms were refined with anisotropic thermal parameters by full-matrix least-squares procedures on F^2. For **1**·0.5 1,4-dioxane, some degree of disorder was observed with carbon atoms of one of the *tert*-butyl groups of the ligand. All the three carbon atoms were displaced over two positions, and they were refined with a site occupation factor of 0.65/0.35, 0.7/0.3, and 0.6/0.4. For **4**·0.5 1,4-dioxane, a similar kind of disorder was observed with carbon atoms of one of the *tert*-butyl groups of the ligand, and they were each refined with a site occupation factor of 0.6/0.4. For **1**·0.5 1,4-dioxane, after anisotropic refinement, unas-

(16) (a) Patra, A. K.; Mukherjee, R. *Inorg. Chem.* **1999**, *38*, 1388–1393. (b) Patra, A. K.; Ray, M.; Mukherjee, R. *Inorg. Chem.* **2000**, *39*, 652–657. (c) Singh, A. K.; Balamurugan, V.; Mukherjee, R *Inorg. Chem.* **2003**, *42*, 6497–6502.

(17) Farrugia, L. J. *WinGX version 1.64, An Integrated System of Windows Programs for the Solution, Refinement and Analysis of Single-Crystal X-ray Diffraction Data*; Department of Chemistry: University of Glasgow, 2003.

Table 1. Data Collection and Structure Refinement Parameters for **1**·0.5 1,4-Dioxane, **2**·2 Diethyl Ether, **3**, and **4**·0.5 1,4-Dioxane

	1·0.5 1,4-Dioxane	**2**·2 Diethyl Ether	**3**	**4**·0.5 1,4-Dioxane
chem formula	$C_{60}H_{76}Co_2N_4O_5$	$C_{66}H_{92}N_4Ni_2O_6$	$C_{58}H_{72}Cu_2N_4O_4$	$C_{60}H_{76}N_4O_6Zn_2$
fw	1051.11	1154.86	1016.28	1079.99
cryst size/mm × mm × mm	0.2 × 0.1 × 0.1	0.2 × 0.1 × 0.1	0.2 × 0.2 × 0.1	0.2 × 0.1 × 0.1
temp/K	100(2)	100(2)	100(2)	100(2)
λ/Å	0.710 69	0.710 73	0.710 69	0.710 69
cryst syst	monoclinic	triclinic	orthorhombic	monoclinic
space group (No.)	*C*2/*c* (15)	*P*-1 (2)	*Aba*2 (41)	*C*2/*c* (15)
a/Å	40.868(5)	9.543(5)	13.677(5)	40.963(5)
b/Å	14.076(5)	17.559(5)	34.017(5)	14.032(5)
c/Å	20.358(5)	19.506(5)	10.880(5)	20.353(5)
α/deg	90	102.504(5)	90	90
β/deg	105.372(5)	103.981(5)	90	105.542(5)
γ/deg	90	90.164(5)	90	90
V/Å^3	11 292(5)	3091(2)	5062(3)	11 271(5)
Z	8	2	4	8
d_{calcd}/g cm^{-3}	1.237	1.241	1.334	1.273
μ/mm^{-1}	0.637	0.662	0.891	0.904
F(000)	4464	1240	2152	4576
no. reflns collcd	37 477	20 791	16 544	37 188
no. unique reflns	13986 (R_{int} = 0.0766)	14707 (R_{int} = 0.063)	5332 (R_{int} = 0.0591)	13875 (R_{int} = 0.1114)
no. reflns used [$I > 2\sigma(I)$]	8668	9090	4470	7718
GOF on F^2	1.094	1.042	1.041	1.043
final *R* indices	0.0742	0.1033	0.0510	0.0842
$[I > 2\sigma(I)]^{a,b}$	0.1911	0.1822	0.1173	0.1961
R indices	0.1243	0.1664	0.0692	0.1575
(all data)^{a,b}	(0.2194)	(0.2286)	(0.1513)	(0.2315)

[a] $R_1 = \Sigma(|F_o| - |F_c|)/\Sigma|F_o|$. [b] $wR_2 = \{\Sigma[w(|F_o|^2 - |F_c|^2)^2]/\Sigma[w(|F_o|^2)^2]\}^{1/2}$.

signed electron density peaks of 1.22 e Å^{-3} and 1.14 e Å^{-3} and for **2**·2 diethyl ether a peak of 1.26 e Å^{-3} were found in the final difference Fourier map, which may be due to the poor quality of crystal chosen for data collection. Pertinent crystallographic parameters are summarized in Table 1.

Theoretical Studies. Calculations were performed using Density Functional Theory (DFT) with Becke's three-parameter hybrid exchange functional[18] and the Lee−Yang−Parr correlation functional (B3LYP).[19] The atomic coordinates of all of the complexes were taken from their X-ray structures. The double-ζ basis set of Hay and Wadt (LanL2DZ) was used for metal centers. The ligand hydrogen, carbon, nitrogen, and oxygen atoms were described using the 6−31G-(d) basis sets. All calculations were performed with the *Gaussian 03* (G03) suite of programs.[20] Orbital diagrams were generated at isosurface of 0.02 using *Gaussview 3.0*.[21]

Results and Discussion

Syntheses of the Ligand and the Complexes. The tripodal ligand 2,4-di*tert*-butyl-6-{[(2-pyridyl)ethyl](2-hydroxybenzyl)aminomethyl}-phenol (H_2L) was synthesized in good yield by condensing 2,4-di*tert*-butyl-6-(chloromethyl)-phenol and 2-((2-(2-pyridinyl)ethylamino)methyl)phenol in the presence of Et_3N in 1,4-dioxane. The ^{1}H NMR spectrum of H_2L is displayed in Figure S1 in the Supporting Information. Notably, this ligand comprises two kinds of phenol units (one unsubstituted and the other one 2,4-di*tert*-butyl-substituted) and a 2-pyridylethylamine moiety. The syntheses of metal complexes were achieved in good yields by reacting appropriate metal salts and H_2L with or without the use of Et_3N. The complex $[Co^{II}_2(L)_2]$·0.5 1,4-dioxane (**1**·0.5 1,4-dioxane) was isolated as a pink powder under refluxing conditions. The complexes $[Ni^{II}_2(L)_2]$ (**2**), $[Cu^{II}_2(L)_2]$ (**3**), and $[Zn^{II}_2(L)_2]$·0.5 1,4-dioxane (**4**·0.5 1,4-dioxane) were isolated as green, brown, and white crystalline solid, respectively. All complexes are readily soluble in CH_2Cl_2. ^{1}H NMR spectrum of diamagnetic **4**·0.5 1,4-dioxane is displayed in Figure S2 in the Supporting Information.

Description of the Structures. To confirm the structure of the complexes, and mode of coordination of the ligand L^{2-}, single crystal X-ray structure determination of the complexes was carried out. Selected bond length, and bond angles are listed in Table 2.

$[Co^{II}_2(L)_2]$·0.5 1,4-Dioxane (1·0.5 1,4-Dioxane). A perspective view of the metal coordination environment in **1**·0.5 1,4-dioxane is shown in Figure 1. The crystal structure reveals a dinuclear complex $[Co^{II}_2(L)_2]$, where the two Co^{II} ions are in a similar five-coordination environment bridged by two phenolate oxygens from two L^{2-} ligands. Each cobalt ion is terminally coordinated by two nitrogens (pyridine and tertiary amine) and a phenolate oxygen of the 2,4-di*tert*-butyl-phenolate ring. Thus, each Co^{II} ion is in a N_2O_3 coordination environment. The equatorial plane of each cobalt(II) ion consists of two phenolate oxygens O(1), O(2) at Co(1), O(3), O(4) at Co(2), and a pyridine nitrogen at

(18) Parr, R. G.; Yang, W. *Density-Functional Theory of Atoms and Molecules*; Oxford University Press: Oxford, U.K., 1989.
(19) (a) Becke, A. D. *J. Chem. Phys.* **1993**, *98*, 5648–5652. (b) Lee, C.; Yang, W.; Parr, R. G. *Phys. Rev. B* **1998**, *37*, 785–789.
(20) Frisch, M. J.; Trucks, G. W.; Schlegel, H. B.; Scuseria, G. E.; Robb, M. A.; Cheeseman, J. R.; Montgomery, J. A.; Vreven, Jr. T.; Kudin, K. N.; Burant, J. C.; Millam, J. M.; Iyengar, S. S.; Tomasi, J.; Barone, V.; Mennucci, B.; Cossi, M.; Scalmani, G.; Rega, N.; Petersson, G. A.; Nakatsuji, H.; Hada, M.; Ehara, M.; Toyota, K.; Fukuda, R.; Hasegawa, J.; Ishida, M.; Nakajima, T.; Honda, Y.; Kitao, O; Nakai, H.; Klene, M.; Li, X.; Knox, J. E.; Hratchian, H. P.; Cross, J. B.; Adamo, C.; Jaramillo, J.; Gomperts, R.; Stratmann, R. E.; Yazyev, O.; Austin, A. J.; Cammi, R.; Pomelli, C.; Ochterski, J. W.; Ayala, P. Y.; Morokuma, K.; Voth, G. A.; Salvador, P. J.; Dannenberg, J.; Zakrzewski, V. G.; Dapprich, S.; Daniels, A. D.; Strain, M. C.; Farkas, O.; Malick, D. K.; Rabuck, A. D.; Raghavachari, K.; Foresman, J. B.; Ortiz, J. V.; Cui, Q.; Baboul, A. G.; Clifford, S.; Cioslowski, J.; Stefanov, B. B.; Liu, G.; Liashenko, A.; Piskorz, P.; Komaromi, I.; Martin, R. L; Fox, D. J.; Keith, T.; Al-Laham, M. A.; Peng, C. Y.; Nanayakkara, A.; Challacombe, M.; Gill P. M. W.; Johnson, B.; Chen, W.; Wong, M. W.; Gonzalez, C.; Pople, J. A. *Gaussian 03*; Gaussian, Inc.: Wallingford, CT, 2004.
(21) Gaussian, Inc.: Wallingford, CT, 2004.

Table 2. Selected Bond Lengths (Angstroms) and Angles (Degrees) in **1**·0.5 1,4-Dioxane, **2**·2 Diethyl Ether, **3**, and **4**·0.5 1,4-Dioxane

		1·0.5 1,4-Dioxane	
Co(1)−O(1)	1.991(2)	Co(1)−O(1)−Co(2)	102.46(11)
Co(1)−O(2)	1.935(3)	Co(1)−O(3)−Co(2)	102.75(11)
Co(1)−O(3)	2.125(3)	O(1)−Co(1)−O(2)	122.03(11)
Co(1)−N(1)	2.183(3)	O(1)−Co(1)−O(3)	76.99(10)
Co(1)−N(2)	2.067(3)	O(1)−Co(1)−N(1)	89.14(11)
Co(2)−O(1)	2.112(3)	O(1)−Co(1)−N(2)	124.30(12)
Co(2)−O(3)	1.969(3)	O(2)−Co(1)−O(3)	103.56(11)
Co(2)−O(4)	1.927(3)	O(2)−Co(1)−N(1)	90.18(12)
Co(2)−N(3)	2.166(3)	O(2)−Co(1)−N(2)	113.66(12)
Co(2)−N(4)	2.118(4)	O(3)−Co(1)−N(1)	164.18(11)
Co(1)Co(2)	3.200(7)	O(3)−Co(1)−N(2)	91.98(12)
		N(1)−Co(1)−N(2)	89.58(13)
		O(1)−Co(2)−O(3)	77.77(10)
		O(1)−Co(2)−O(4)	88.13(11)
		O(1)−Co(2)−N(3)	169.99(11)
		O(1)−Co(2)−N(4)	95.31(13)
		O(3)−Co(2)−O(4)	120.59(12)
		O(3)−Co(2)−N(3)	93.11(11)
		O(3)−Co(2)−N(4)	101.29(13)
		O(4)−Co(2)−N(3)	91.33(12)
		O(4)−Co(2)−N(4)	137.65(13)
		N(3)−Co(2)−N(4)	92.50(14)
		2·2 Diethyl Ether	
Ni(1)−O(1)	2.002(4)	Ni(1)−O(1)−Ni(1)^a	100.78(17)
Ni(1)−O(2)	1.937(4)	O(1)−Ni(1)−O(2)	130.22(18)
Ni(1)−O(1)^a	2.058(4)	O(1)−Ni(1)−O(1)^a	79.22(18)
Ni(1)−N(1)	2.084(5)	O(1)−Ni(1)−N(1)	95.10(19)
Ni(1)−N(2)	2.035(5)	O(1)−Ni(1)−N(2)	94.20(19)
Ni(1)Ni(1)^a	3.151(8)	O(2)−Ni(1)−O(1)^a	89.78(17)
		O(2)−Ni(1)−N(1)	92.73(19)
		O(2)−Ni(1)−N(2)	135.08(19)
		O(1)^a−Ni(1)−N(1)	174.09(19)
		O(1)^a−Ni(1)−N(2)	93.00(18)
		N(1)−Ni(1)−N(2)	89.0(2)
		3	
Cu(1)−O(1)	1.962(3)	Cu(1)−O(1)−Cu(1)^a	101.06(13)
Cu(1)−O(2)	1.892(3)	O(1)−Cu(1)−O(2)	160.56(14)
Cu(1)−O(1)^a	1.992(3)	O(1)−Cu(1)−O(1)^a	74.04(14)
Cu(1)−N(1)	2.050(4)	O(1)−Cu(1)−N(1)	94.77(14)
Cu(1)−N(2)	2.245(4)	O(1)−Cu(1)−N(2)	98.59(14)
Cu(1)Cu(1)^a	3.053(4)	O(2)−Cu(1)−O(1)^a	91.52(13)
		O(2)−Cu(1)−N(1)	95.01(15)
		O(2)−Cu(1)−N(2)	97.95(15)
		O(1)^a−Cu(1)−N(1)	160.18(15)
		O(1)^a−Cu(1)−N(2)	106.36(14)
		N(1)−Cu(1)−N(2)	91.27(15)
		4·0.5 1,4-Dioxane	
Zn(1)−O(1)	2.019(3)	Zn(1)−O(1)−Zn(2)	103.37(14)
Zn(1)−O(2)	1.942(3)	Zn(1)−O(3)−Zn(2)	103.29(14)
Zn(1)−O(3)	2.118(3)	O(1)−Zn(1)−O(2)	122.06(14)
Zn(1)−N(1)	2.187(4)	O(1)−Zn(1)−O(3)	76.07(13)
Zn(1)−N(2)	2.076(4)	O(1)−Zn(1)−N(1)	88.81(14)
Zn(2)−O(1)	2.091(3)	O(1)−Zn(1)−N(2)	123.13(15)
Zn(2)−O(3)	1.994(3)	O(2)−Zn(1)−O(3)	103.58(14)
Zn(2)−O(4)	1.940(3)	O(2)−Zn(1)−N(1)	91.68(15)
Zn(2)−N(3)	2.164(5)	O(2)−Zn(1)−N(2)	114.81(15)
Zn(2)−N(4)	2.133(5)	O(3)−Zn(1)−N(1)	162.59(14)
Zn(1)Zn(2)	3.226(7)	O(3)−Zn(1)−N(2)	90.72(15)
		N(1)−Zn(1)−N(2)	90.39(16)
		O(1)−Zn(2)−O(3)	77.22(13)
		O(1)−Zn(2)−O(4)	89.05(14)
		O(1)−Zn(2)−N(3)	168.63(15)
		O(1)−Zn(2)−N(4)	93.72(17)
		O(3)−Zn(2)−O(4)	123.02(15)
		O(3)−Zn(2)−N(3)	92.70(15)
		O(3)−Zn(2)−N(4)	100.82(17)
		O(4)−Zn(2)−N(3)	92.15(16)
		O(4)−Zn(2)−N(4)	135.46(17)
		N(3)−Zn(2)−N(4)	93.34(19)

^{a} Symmetry operator for the generated atoms: $-x+1, -y, -z+1$ for **2**·2 Diethyl Ether and $-x+2, -y, z$ for **3**.

Figure 1. A perspective view of $[Co^{II}_2(L)_2]$ in the crystal of $[Co^{II}_2(L)_2]$·0.5 1,4-Dioxane (**1**·0.5 1,4-Dioxane). Only donor atoms are labeled. Hydrogen atoms and uncoordinated solvent molecules are omitted for clarity.

N(2) and N(4). The axial positions are occupied by a phenolate oxygen O(3) and an amine nitrogen N(1) at Co(1), O(1), and N(3) at Co(2). Thus, the geometry around the two cobalt(II) ions is distorted trigonal-bipyramidal [$\tau = 0.66$ for Co(1) and 0.52 for Co(2)].[22] Whereas Co(1) is positioned out of the equatorial plane toward O(3) by 0.013(3) Å, Co(2) is positioned out of the equatorial plane toward N(3) by 0.077(4) Å. The Co_2O_2 core is almost planar [the angle between the two planes passing through the atoms Co(1)−O(1)−Co(2), and Co(1)−O(3)−Co(2) is 2.08(15)°]. Because of the expected difference in bond length between axial and equatorial coordination, the Co(1)−O(1) and Co(2)−O(3) bonds are shorter than the Co(1)−O(3) and Co(2)−O(1) bonds, attesting to the asymmetrical nature of the Co_2O_2 core. The two cobalt(II) centers are separated by 3.200(7) Å, which is similar to the other phenoxo-bridged dinuclear cobalt(II) complexes.[23] Between the two $Co-O_{phenolate}$ bond distances in the equatorial plane, the substituted phenolate ring coordinates more effectively than the unsubstituted phenolate.

$[Ni^{II}_2(L)_2]$·2 Diethyl Ether (2·2 Diethyl Ether). The molecular structure of $[Ni^{II}_2(L)_2]$ is shown in Figure S3 in the Supporting Information. The molecule sits on a crystallographically imposed center of inversion, forming the bridged dinuclear structure with each nickel being five-coordinate, sharing two phenolate oxygens from two ligands. The terminal coordination around each nickel(II) ion is similar to that in **1**·0.5 1,4-dioxane. The dispositions of donor atoms in the equatorial and axial positions are similar to that in **1**·0.5 1,4-dioxane. The geometry around each nickel(II) center is distorted trigonal-bipyramidal (τ value, 0.65).[22] The Ni_2O_2 core is planar, as dictated by symmetry. However, the bridge is again slightly asymmetric. The distance between the two nickel(II) centers is 3.151(8) Å. The nickel(II) ion is positioned out of the equatorial plane toward the N(1) atom by 0.078(4) Å. The trends of other metric parameters are similar to that in **1**·0.5 1,4-dioxane. Generally, the metric

(22) Addison, A. W.; Rao, T. N.; Reedjik, J.; van Rijn, J.; Vershcoor, G. C. *J. Chem. Soc., Dalton Trans.* **1984**, 1349–1356.
(23) Rodríguez, L.; Labisbal, E.; Sousa-Pedrares, A; García-Vázquez, J. A.; Romero, J.; Durán, M. L.; Real, J. A.; Sousa, A. *Inorg. Chem.* **2006**, *45*, 7903–7914.

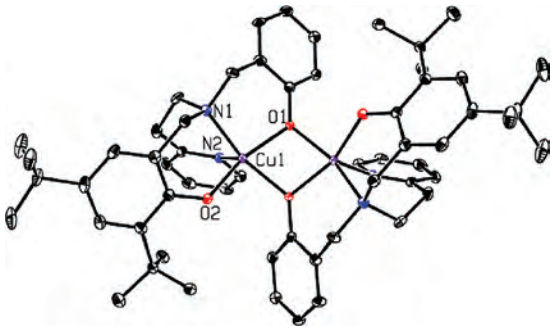

Figure 2. A perspective view of the crystal structure of $[Cu^{II}_2(L)_2]$ (**3**). Only donor atoms are labeled. Hydrogen atoms are omitted for clarity.

parameters are comparable with other diphenoxo-bridged nickel(II) complexes.[24]

$[Cu^{II}_2(L)_2]$ (3). The asymmetric unit contains two independent molecules, and each molecule sits on a crystallographically imposed inversion center. The molecular structure of $[Cu^{II}_2(L)_2]$ is shown in Figure 2. In contrast to the structures of **1**·0.5 1,4-dioxane and **2**·2 diethyl ether, here each copper(II) ion is in perfect square-pyramidal geometry (τ value, 0.006),[22] the ethylpyridine nitrogen N(2) acts as the axial ligand, and the basal plane consists of three phenolate oxygens O(1), O(2), and O(1)*, and an amine nitrogen N(1). As a consequence, the Cu_2O_2 core is twisted toward a butterfly shape [the dihedral angle between the two planes passing through the atoms Cu(1)−O(1)−Cu(1)*, and Cu(1)−O(1)*−Cu(1)* is 37.80(17)°], leading to a Cu(1)···Cu(1)* distance of 3.053(4) Å. The copper(II)−phenolate distances are comparable to other diphenoxo-bridged complexes.[6d,f,8a,e,9,11,25,26]

$[Zn^{II}_2(L)_2]$·0.5 1,4-Dioxane (4·0.5 1,4-Dioxane). The molecular structure of $[Zn^{II}_2(L)_2]$ is shown in Figure S4 in the Supporting Information. The structure is closely similar to those of **1**·0.5 1,4-dioxane. The Zn_2O_2 core is almost planar with a dihedral angle [between the two planes passing through the atoms Zn(1)−O(1)−Zn(2) and Zn(1)−O(2)−Zn(2)] of 2.89(15)°. However, the bridge is slightly asymmetric. The bonding parameters are closely similar to that observed in **1**·0.5 1,4-dioxane. The distance between the two zinc(II) centers is 3.226(7) Å, which is similar to the other phenoxo-bridged dinuclear zinc(II) complexes.[8f,27] The geometry around the two zinc(II) ions is distorted trigonal-bipyramidal, with τ values of 0.66 for Zn(1) and 0.55 for Zn(2).[22]

Absorption Spectra. Absorption spectral analyses (below) of **1**·0.5 1,4-dioxane, **2**, and **3** in CH_2Cl_2 clearly support the presence of five-coordinate cobalt(II), nickel(II), and copper(II). The electronic spectrum of **1**·0.5 1,4-dioxane exhibits d−d transitions at 570, and 740 nm with ϵ = 200 and 30 M^{-1} cm^{-1}, respectively,[23] and a shoulder at 380 nm (ϵ = 2900 M^{-1} cm^{-1}) (Figure S5 in the Supporting Information) that is attributed to a phenolate-to-cobalt(II) charge-transfer transition.[28] For **2**, the phenolate-to-nickel(II) charge-transfer transition is observed at 420 nm (ϵ = 3200 M^{-1} cm^{-1}), and d−d bands are at 670 and 970 nm with ϵ = 60 and 20 M^{-1} cm^{-1}, respectively (Figure S6 in the Supporting Information). Similar features were observed for a closely similar complex.[7e] The intense brown color of **3** suggests the presence of strong phenolate-to-copper(II) charge-transfer transition at 390 nm (ϵ = 3400 M^{-1} cm^{-1}), along with a shoulder at 510 nm (ϵ = 2200 M^{-1} cm^{-1}). The weak band at 760 nm is associated with a d−d transition of a square-based copper(II) center[25] (Figure S7 in the Supporting Information). Intraligand transitions are displayed at still higher energies for **1**·0.5 1,4-dioxane, **2**, and **3** at 290 nm.

Magnetism. To extract information about the nature and extent of magnetic exchange interaction between the two metal centers, temperature-dependent (2−300 K) magnetic susceptibility measurements on powder samples of **1**·0.5 1,4-dioxane, **2**, and **3** were carried out. The values of $\chi_M T$ at room temperature are 4.80 (**1**·0.5 1,4-dioxane), 2.08 (**2**), and 0.43 cm^3 mol^{-1} K (**3**). Because of their dinuclear nature, the experimental data were modeled using the Hamiltonian, with $S_1 = S_2 = {}^3/_2$ (**1**·0.5 1,4-dioxane), 1 (**2**), and ${}^1/_2$ (**3**). To reduce the number of variables, D (zero-field splitting parameter) and g values ($g_z = g_x = g_y$) were considered to be identical for the two metal ions.[29] It should be mentioned, however, that the local zero-field splitting corresponding to the Hamiltonian term was not considered in the case of **3**. Satisfactory fits were obtained: g = 2.27(1) and D = 7.7(2) cm^{-1}, and J = −6.1(2) cm^{-1} for **1**·0.5 1,4-dioxane (Figure S8 in the Supporting Information);[29,30a] g = 2.15(1) and D = 4.5(2) cm^{-1}, and J = −28.6(3) cm^{-1} for **2** (Figure S9 in the Supporting Information);[25,29,30b] g = 2.12(1) and J = −359(2) cm^{-1} for **3** (Figure 3).[23,25,26,29] Thus the dimetal(II) centers in these complexes are antiferromagnetically coupled.

Redox Properties. To investigate the possibility of observing metal-coordinated 2,4-di*tert*-butyl-phenolate ring oxidation(s), the cyclic voltammograms (CV) of all four complexes were recorded in CH_2Cl_2 at a scan rate of 100 mVs^{-1}, using a platinum working electrode. Each complex displays two quasireversible one-electron oxidative responses at $E_{1/2}{}^1$ = 0.57 (**1**·0.5 1,4-dioxane), 0.52 (**2**), 0.50 (**3**), and 0.58 (**4**·0.5 1,4-dioxane) and $E_{1/2}{}^2$ = 0.70 (**1**·0.5 1,4-dioxane), 0.63 (**2**), 0.64 (**3**), and 0.75 (**4**·0.5 1,4-dioxane) V vs SCE. The CV scans of **1**·0.5 1,4-dioxane, **2**, **3**, and **4**·0.5 1,4-dioxane are displayed in Figure S10 (Supporting Information), Figure S11 (Supporting Information), Figure 4, and Figure S12 (Supporting Information), respectively. Because of the invariant nature of the $E_{1/2}$ values we assign the

(24) Pal Chaudhuri, U.; Varghese, B.; Murthy, N. N. *Acta Crystallogr.* **2003**, *E59*, m627–m629.
(25) Gupta, R.; Mukherjee, S.; Mukherjee, R *J. Chem. Soc., Dalton Trans.* **1999**, *402*, 5–4030.
(26) Mukherjee, R. Chapter on Copper. In *Comprehensive Coodination Chemistry-II: From Biology to Nanotechnology*; McCleverty, J. A., Meyer, T. J., Fenton, D. E., Eds.; Elsevier/Pergamon: Amsterdam, 2004; pp 747−910.
(27) (a) Reglinski, J.; Morris, S.; Stevenson, D. E. *Polyhedron* **2002**, *21*, 2175–2182. (b) Matalobos, J. S.; Garcβa-Deibe, A. M.; Fondo, M.; Navarro, D.; Bermejo, M. R. *Inorg. Chem. Commun.* **2004**, *7*, 311–314.
(28) Du, M.; An, D.-L.; Guo, Y.-M.; Bu, X.-H. *J. Mol. Struct.* **2002**, *641*, 193–198.
(29) Details of magnetic behavior from the standpoint of magneto-structural correlation will be published elsewhere.
(30) (a) Mishra, V.; Lloret, F.; Mukherjee, R. *Inorg. Chim. Acta* **2006**, *359*, 4053–4062. (b) Mishra, V.; Lloret, F.; Mukherjee, R. *Eur. J. Inorg. Chem.* **2007**, 2161–2170.

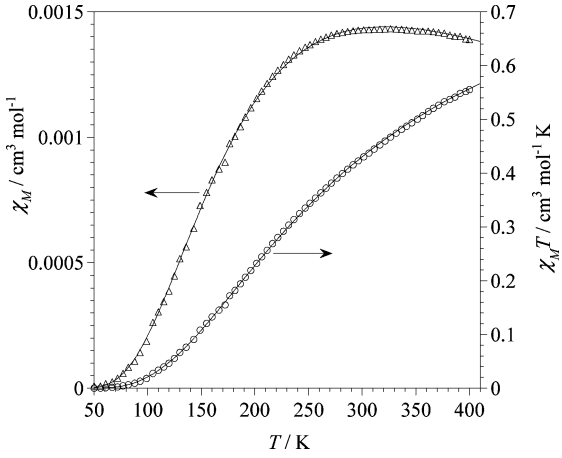

Figure 3. Plots of χ_M vs T (left scale) and $\chi_M T$ vs T (right scale) for a powdered sample of **3**. The solid lines represent the best theoretical fit, described in the text.

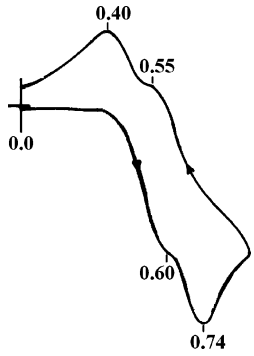

Figure 4. Cyclic voltammogram (100 mV/s) of a ~1.0 mM solution of **3** at a platinum electrode in CH_2Cl_2 (0.1 M in TBAP). Indicated potentials (in V) are vs SCE.

oxidative responses presumably due to a successive oxidation of coordinated 2,4-di*tert*-butyl-phenolate rings into phenoxyl radicals (ligand-centered oxidations, below).

Nature of Two-Electron Oxidized Species. Coulometrically generated two-electron oxidized species of **1**·0.5 1,4-dioxane and **2** are not stable enough to allow their redox (lack of well-defined redox response) and spectroscopic (featureless UV−vis spectra and lack of EPR signal) characterization. Whether or not there is a possibility of formation of monomeric/dimeric Co^{III}−phenolate/phenoxyl radical complex,[7g] we attempted to synthesize such a compound.[31] To extract information about the stability of oxidized species of **3** and **4**·0.5 1,4-dioxane in CH_2Cl_2, we investigated the time course of spectral change during decay. The results are displayed in Figure S13 (Supporting Information) and Figure S14 (Supporting Information), respectively. Therefore, two-electron oxidized solutions of **3** ($k_{decay} = 3.6821 \times 10^{-1}$ min^{-1}; $t_{1/2} \approx 1.88$ min) and **4**·0.5 1,4-dioxane ($k_{decay} = 3.1042 \times 10^{-1}$ min^{-1}; $t_{1/2} \approx 2.23$ min) allowed us to investigate the nature of oxidized species in reasonable detail (below). Similar values were reported for monomeric copper(II) complexes with a N_2O_2 donor set.[6d] Notably, no change of decay behavior was observed even at 223 K.

Notably, the $E_{1/2}$ values of two consecutive oxidative responses (above) and the energies of the HOMOs for **2** and **3** (Table 3) are similar, but the stability of their two-electron oxidized product is different. We believe that comparatively greater stability in the case of **3** may arise due to spin-pairing between the unpaired electron on the phenoxyl radical and that on the d^9 metal center.[10d] Understandably, the presence of an additional unpaired electron at each metal center in the case of **2** cannot allow such a spin-pairing, which in turn might have contributed to its instability.

The electronic spectrum of the oxidized species, generated by electrolysis of CH_2Cl_2 solutions (containing 0.1 M TBAP as supporting electrolyte) at 298 K, of **3** [applied potential: 0.90 V vs SCE, $n = 1.90$, color change: reddish brown to light yellowish brown] exhibits characteristic bands at 420 nm ($\epsilon = 1600$ M^{-1} cm^{-1}), and at 770 nm ($\epsilon = 470$ M^{-1} cm^{-1}) (Figure 5). This species was also generated in CH_2Cl_2 by chemical oxidation (AgOTf). The CV scan (starting potential, 1.00 V) of such oxidized solutions display a reductive response (cathodic peak potential, $E_{pc} = 0.06$ V and a stripping peak at 0.36 V), which is typical for a monomeric copper(II) species (Figure S15, Supporting Information). **3** is EPR-silent due to strong antiferromagnetic exchange coupling between the two copper(II) centers mediated by the diphenoxo-bridge (above). However, the X-band EPR spectrum of the product of two-electron oxidation exhibits an axial signal at $g_{||} = 2.27$, $g_{\perp} = 2.05$, and $A_{||} = 161 \times 10^{-4}$ cm^{-1}, which is typical for monomeric copper(II) (Figure 5). No EPR signal centered at $g \sim 4$, associated with $\Delta M_s = \pm 1$ transition typical of an $S = 1$ system (ferromagnetic coupling between the phenoxyl radical and the copper(II) center) was observed.

On the basis of the above observations, we speculate that after two-electron oxidation, **3** is converted to a monomeric Cu^{II}−phenolate−phenoxyl radical species, which instantaneously abstracts the hydrogen atom[8d] (we are not in a position to identify the source; however, a solvent or trace of moisture present in solvent is a possibility), and forms a monomeric Cu^{II}−phenolate−phenol species.[1i,5a,6g] It should be mentioned here that the coordinated ligand remained intact during the course of this reaction, as judged by mass (Figure S16, Supporting Information) and ^{1}H NMR (Figure S17, Supporting Information) spectra of the extracted organic component after removal of copper by aqueous ammonia from such solutions. Notably, addition of 2 equiv of Et_3N to chemically/coulometrically oxidized solutions of **3** quantitatively regenerates **3** (below), implying the presence of an acidic proton in such a copper(II) complex. If our proposition is right, then addition of 2 equiv of $HClO_4$ to **3** is expected to generate a Cu^{II}−phenolate−phenol species, as before. In fact, exactly such a reaction sequence was implicated by an optical titration. Figure 6 displays such an optical titration at 298 K of dimeric **3** with 2 equiv of $HClO_4$, followed by the addition of 2 equiv of Et_3N and regeneration of dimer **3**. This result strengthens our proposition of hydrogen-atom abstraction and the existence of a monomeric Cu^{II}−phenolate−phenol complex (Scheme 1). The Cu^{II}−phenolate−phenol

(31) A mixed-ligand complex of composition [Co^{III}(L)(acac)] (acac = acetylacetonate anion) has been isolated. This complex allows coulometric generation of a Co^{III}−phenoxyl radical species. Details of this chemistry will be published elsewhere.

Table 3. Results of DFT Calculation

	Composition of HOMO			
complexes	energy of HOMO (kcal/mol)	contribution (%) from 2,4-di*tert*-butyl phenolate ring	total contribution (%) from ligand	contribution (%) from metal ion
$[Co^{II}_2(L)_2]$ (**1**)	−101.15	48	91	6
$[Ni^{II}_2(L)_2]$ (**2**)	−104.16	52	93	3
$[Cu^{II}_2(L)_2]$ (**3**)	−105.00	37	90	6
$[Zn^{II}_2(L)_2]$ (**4**)	−91.85	56	94	4

complex is expected to exhibit higher[6d,e] $Cu^{II}-Cu^{I}$ redox potential (cathodic peak potential, $E_{pc} = 0.06$ V vs SCE; Figure S15, Supporting Information) than that of the monomeric complex $[Cu^{II}(L)(DMF)]$ [$E_{pc} = -1.08$ V vs SCE].[32] The species responsible for the reductive CV scan (Figure S15, Supporting Information), and EPR spectra (Figure 5) of coulometrically oxidized CH_2Cl_2 solutions is thus of the Cu^{II}−phenolate−phenol complex.

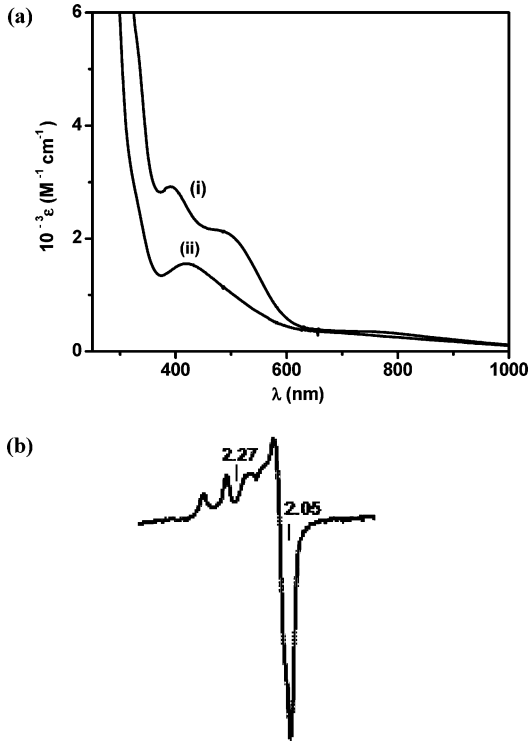

Figure 5. (a) Absorption spectra (CH_2Cl_2 solution) of (i) **3** and (ii) its coulometrically generated two-electron oxidized species. The ε values are based on dimer composition; (b) X-band EPR spectrum (CH_2Cl_2, 120 K) of coulometrically generated two-electron oxidized species of **3**.

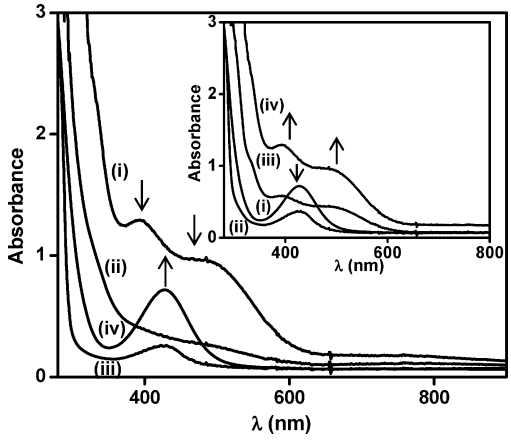

Figure 6. Titration of **3** (0.4 mM in CH_2Cl_2) by H^+ ($HClO_4$). Arrows indicate the direction of absorption change with increasing H^+ ion concentration: (i) initial solution of **3** and (ii)−(iv) after the addition of 0.2, 0.5, and 2.0 equiv of $HClO_4$, respectively. Titration of the Cu^{II}−phenolate−phenol species by Et_3N is displayed as an inset. Arrows indicate the direction of absorption change with increasing Et_3N concentration: (i) initial solution and (ii)−(iv) after the addition of 0.2, 0.5, and 2.0 equiv of Et_3N, respectively.

The electronic spectrum of the oxidized species of **4**·0.5 1,4-dioxane [applied potential, 1.00 V vs SCE, $n = 1.95$; color change, colorless to orangish yellow] exhibits a band at 430 nm ($\epsilon = 700$ M^{-1} cm^{-1}) attributed to the $\pi-\pi^*$ transition of a phenoxyl radical and another absorption at 840 nm ($\epsilon = 60$ M^{-1} cm^{-1}) (Figure 7). The transition at 840 nm could arise from ligand-based transitions and/or a ligand → ligand charge-transfer (LLCT) transition.[10b] After oxidation, its dimeric structure is retained, as such solutions display two reductive responses at the same potentials as those observed for **4**·0.5 1,4-dioxane (Figure S15, Supporting Information). Notably, such solutions in its X-band EPR spectrum exhibit an isotropic signal at $g = 2.006$, typical for phenoxyl radical species (Figure 7). The interaction between the two phenoxyl moieties is thus very weak, meaning thereby the localization of the radicals.[6h] So, from the spectral feature of two-electron oxidized species of **4**·0.5 1,4-dioxane, we confirm that the observed redox responses are due to Zn^{II}-coordinated ligand-centered oxidations. It is worth noting here that contrary to that observed for **4**·0.5 1,4-dioxane, after two-electron oxidation of **3** the generated copper(II)−phenolate−phenoxyl radical species instantaneously rearranges to copper(II)−phenolate−phenol complex. The reason behind differential stability of two oxidized species generated from **3** and **4**·0.5 1,4-dioxane must be due to the relative stability of one species over another [cf. Figure S13 and Figure S14, Supporting Information; $t_{1/2}$ (**3**) ≈ 1.88 min and $t_{1/2}$ (**4**·0.5 1,4-dioxane) ≈ 2.23 min].

Computational Results. To get an idea about the site of oxidation, we performed single-point DFT calculations at the B3LYP level of theory on all four complexes using their X-ray crystallographic coordinates. In each case, analysis of the HOMO reveals that it is predominantly contributed by ligand orbitals. The maximum contribution comes from the 2,4-di*tert*-butyl-phenolate part of the ligand, and there is very little contribution of the metal center. The HOMO of each complex is delocalized over the *tert*-butyl phenol ring of the

(32) A mononuclear copper(II) complex of composition $[Cu^{II}(L)(DMF)]$ has been isolated. Characterization has been done by mass spectral analysis at m/z = 581.09 [Calcd for $(C_{32}H_{43}N_3CuO_3 + 1)^+ = 581.50$]. UV-vis [$\lambda$, nm ($\varepsilon$, M^{-1} cm^{-1}), in DMF]: 450 (1650) and 750 (200). EPR (solid, 298 K): $g_{\|} = 2.27$, $g_{\perp} = 2.07$, and $A_{\|} = 174 \times 10^{-4}$ cm^{-1}. Details of this chemistry will be published elsewhere.

Scheme 1. Coulometrically-generated phenoxyl radical-coordinated dicopper(II) complex transforms to a monomeric complex with instantaneous abstraction of hydrogen atoms. The trace amount of water present in CH_2Cl_2 might provide fifth coordination to the copper(II) center

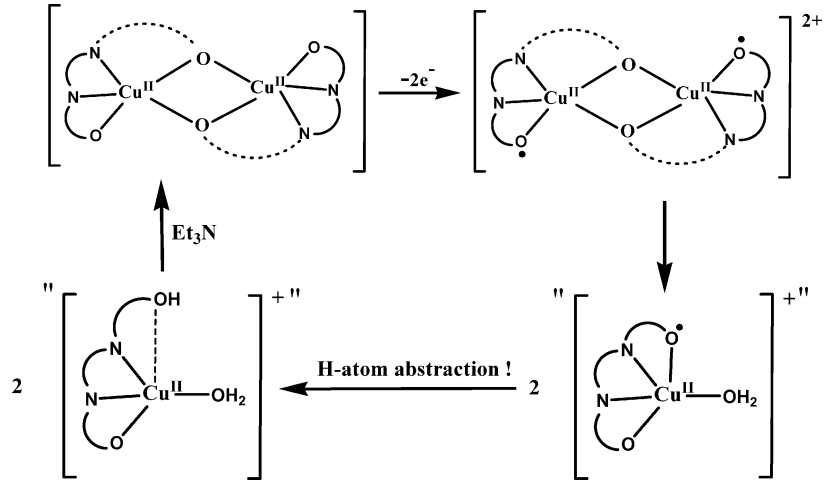

ligand, with the contribution from the phenolic oxygen atom. The results for **1**, **2**, **3**, and **4** are in Figure S18 (Supporting Information), Figure 8, and Figure S19 (Supporting Information), respectively. Quantitative evaluations of the atomic orbital contributions to the relevant HOMOs and the energy of the HOMOs are summarized in Table 3.

Summary and Concluding Remarks

From the perspective of recent emergence of free radical enzymology in this article, we successfully combined the merits of a new tripodal ligand [comprising two phenol groups (one unsubstituted and the other with 2,4-di*tert*-butyl substituents), an ethylpyridine unit, and an aliphatic amine] and different metal ions to synthesize four diphenoxo-bridged dimetal(II) complexes, with each metal center having a N_2O_3 coordination environment. Comparing the structures of the complexes, we found that cobalt(II), nickel(II), and zinc(II) have distorted trigonal-bipyramidal geometry, and copper(II) has perfect square-pyramidal geometry. Each ligand provides a phenoxo bridge by its unsubstituted phenolate group. The successful preparation and systematic investigation of properties of four closely similar complexes provide a valuable source of information for the understanding of their structures, magnetic properties, and redox behavior (each complex exhibits two successive oxidations at closely similar potentials). Out of the two phenolate groups present in the ligand, the one with the 2,4-di*tert*-butyl substituent is oxidized, as suggested by the composition of HOMOs of the complexes (DFT calculations at the B3LYP level of theory). In essence, the present study gives a lot of insights into the properties

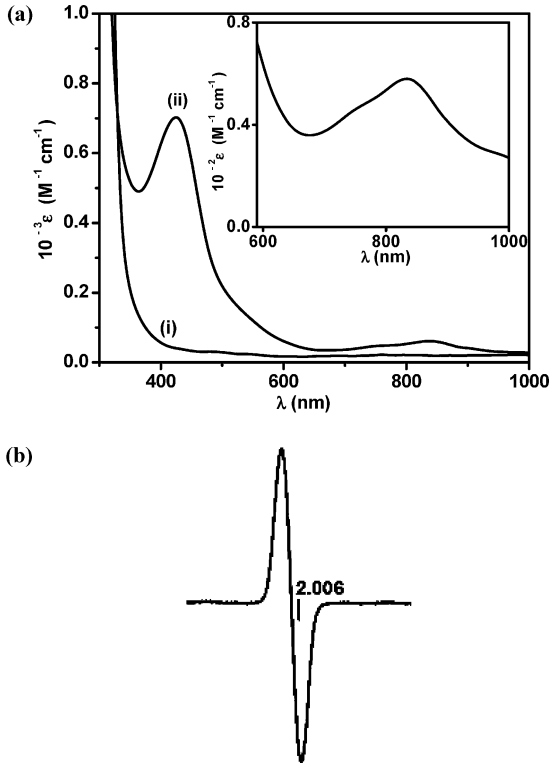

Figure 7. (a) Absorption spectra (CH_2Cl_2 solution) of (i) **4**·0.5 1,4-dioxane, and (ii) its coulometrically generated two-electron oxidized species. The enlarged feature between 600−1000 nm is shown as an inset. (b) X-band EPR spectrum (CH_2Cl_2, 120 K) of coulometrically generated two-electron oxidized species of **4**·0.5 1,4-dioxane.

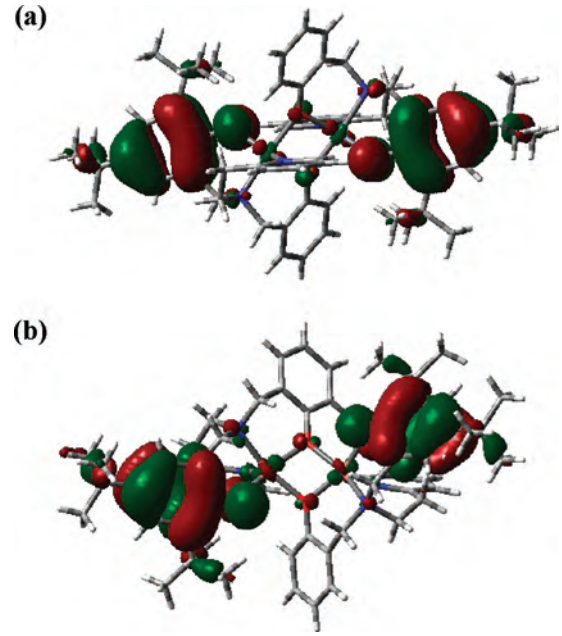

Figure 8. Contour plots of the HOMO of (a) **2** and (b) **3**.

of metal-coordinated phenoxyl radicals that play an important role not only in the enzymatic systems but also in the catalytic processes in several organic reactions. Efforts are underway to stabilize metal-coordinated phenoxyl radical complexes in general and a Ni^{II}−phenoxyl radical species in particular.

Acknowledgment. This work is supported by grants from the Council of Scientific and Industerial Research, and Department of Science and Technology, Government of India, New Delhi. R.M. sincerely thanks Prof. Dan Stack (Department of Chemistry, Stanford University) for arousing his interest in DFT calculation during the author's stay (sabbatical leave 2005−2006) in the laboratory of Prof. Stack. R.M. also wishes to express his thanks to Dr. Tim Storr and Mr. Pratik Verma (Stanford University). A.M. sincerely thanks Ms. Nabanita Sadhu Khan (Department of Chemistry, IIT Kanpur) for her help in DFT calculations. Comments of the reviewers were very helpful at the revision stage.

Supporting Information Available: ^{1}H NMR spectra of H_2L and **4**·0.5 1,4-dioxane in $CDCl_3$; perspective views of **2**·2 diethyl ether and **4**·0.5 1,4-dioxane; absorption spectra of **1**·0.5 1,4-dioxane, **2**, and **3** in CH_2Cl_2; plot of $\chi_M T$ vs T for **1**·0.5 1,4-dioxane, **2**; CV scans in CH_2Cl_2 of **1**·0.5 1,4-dioxane, **2**, and **4**·0.5 1,4-dioxane; time-course of spectral change of the two-electron oxidized species of **3**, and **4**·0.5 1,4-dioxane in CH_2Cl_2; CV scans of coulometrically generated two-electron oxidized species of **3** and **4**·0.5 1,4-dioxane in CH_2Cl_2; mass, and ^{1}H NMR in $CDCl_3$ of two-electron oxidized species of **3**, after removal of copper by aqueous ammonia; HOMO and HOMO-1 contour plots of **1**, and **4**. CIF files for **1**·0.5 1,4-dioxane, **2**·2 diethyl ether, **3**, and **4**·0.5 1,4-dioxane. This material is available free of charge via the Internet at http://pubs.acs.org.

IC701283B